Detecting permafrost landscape changes in northern Alaska and the Mackenzie River Delta with Landsat Data

[1]Humboldt-Universität zu Berlin

Contents

List of Figures

List of Tables

Abstract. With the onset of global climate change, Earth's permafrost regions are of particular interest, since approximately 50% of the global subsurface carbon reservoir is located in the Arctic permafrost region (Hollesen et al., 2015). Thawing permafrost and the release of carbon to the atmosphere triggered by rising temperatures and changing weather patterns is considered as a potential tipping point and a global-scale positive feedback on climate change (Hollesen et al., 2015). Due to their remoteness, adequate monitoring of these regions is sometimes very difficult. Methods employing remote sensing techniques using trend analysis are an effective way to tackle these challenges. In this study we are using the Landsat archive to identify change processes in the North American Arctic coast employing a trend analysis process based on research by Nitze and Grosse (2016). In addition, the extent of these processes were estimated based on the trend data and a general change classification was undertaken. We confirmed the results of increased greening of the permafrost tundra between 1999 and 2014 and identified processes causing the trends. Google Earth Engine was used as a processing infrastructure which proved to be an excellent platform to conduct these kinds of analyses.

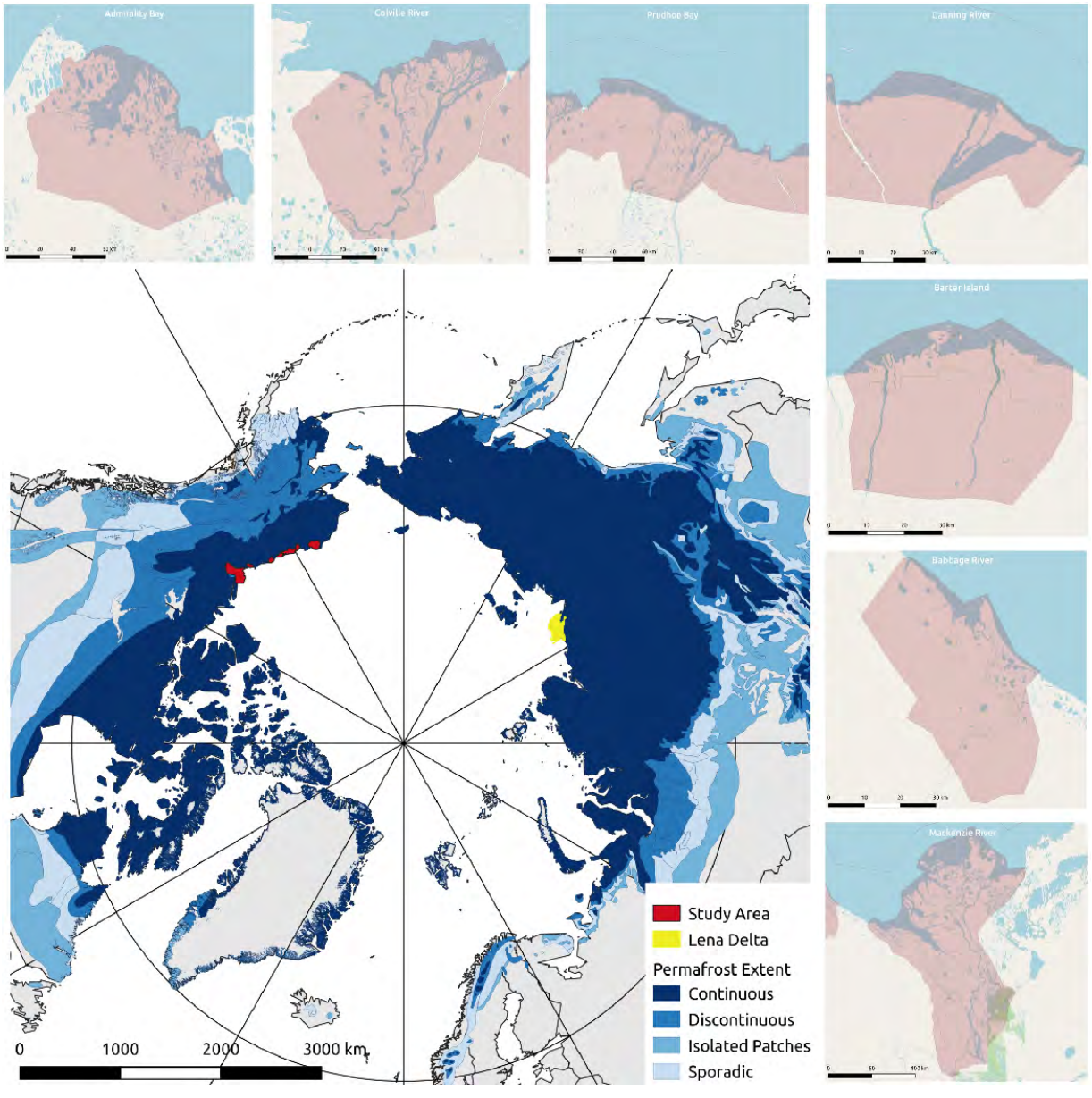

Figure 1. The figure shows an overview map with permafrost extent, study areas in red and the Lena River delta in yellow (Permafrost Map based on: Brown et al. (1998)). The seven study regions are displayed in more detail in the smaller maps (Basemaps are based on: OpenStreetMap contributors (2017).

1 Introduction

Climate change affects multiple regions worldwide, with changing precipitation patterns, increasing intensity and frequency of extreme weather events and increasing temperatures (IPCC, 2019). The effect is especially pronounced in the Arctic regions through feedback patterns, denoted as "arctic amplification" (Serreze and Barry, 2011). Arctic permafrost regions are therefore exposed to increasing mean temperature and longer thawing seasons, which affects the active layer depth and bounding properties of the soil. Permafrost degradation due to these processes affect local fauna and flora, destroy built-up infrastructure (Hjort et al., 2018) and induce the release of potent greenhouse gases bound in the frozen soil, creating a positive feedback loop through further increasing temperatures (IPCC, 2019; Berner et al., 2020; Nitzbon et al., 2020).

Understanding these processes and monitoring the effects is crucial in predicting permafrost development in the near future and estimating the sensitivity of the whole earth system to climate change. As permafrost regions are often at remote locations with little infrastructure for local monitoring, remote sensing techniques are applied to derive information from data acquired by air or space-borne sensors (Markon et al., 1995; Berner et al., 2020). Beginning in the 1970s, an increasing number of earth observation satellites provide global monitoring with increasing spatial and temporal resolution (Wulder et al., 2016).

Several methods to transform raw reflectance data into evidence for surface change processes were derived and applied to the permafrost regions. Indexed metrics derived from the surface reflectance were employed to create time series and identify changes in the permafrost structure (Markon et al., 1995; Beck et al., 2015). Time series data can further be condensed into trend analysis, where data from multiple data points in a time period are reduced to simple trend evaluations with statistical analysis through regression models (e.g. Fraser et al., 2014).

Nitze and Grosse (2016) employed the Theil-Sen regression (TSR) algorithm to extract Tasseled Cap and multiple normalized difference index trends from Landsat data in the Lena Delta region in Siberia. They found noticeable increased greening and surface wetness trends near coastal areas, ice-rich permafrost or major channels of the delta.

This report employs the same methods to study permafrost change processes at river deltas in the permafrost region of North Slope, Alaska. In addition to investigating the feasibility of applying Nitze and Grosse's methods in other regions, this study focuses on the following questions:

- Is the magnitude of trends comparable to the results of Nitze and Grosse (2016) and can similar processes be found?
- Can the trend analysis help to identify local change processes in the permafrost and what is the areal extent of these processes?
- Are trend data a feasible base to create supervised change process classifications?

2 Study Site

Six regions with river deltas in North Slope, Alaska and the MacKenzie River Delta in northern Canada (Figure 1) were delineated in Google Earth Pro to represent different types of coastal morphology while still being comparable to the Lena Delta of the original study. The rough delineations include barrier islands close to the coast to examine trends caused by marine erosion and sedimentation.

Three regions (Admirality Bay, Colville River and Prudhoe Bay) exhibit large areas dominated by thermokarst lakes. Canning River represents rivers creating alluvial fans across the coastline with less delta formation. The Barter Island and Babbage River regions contain large alluvial plains, with a pronounced birdfoot delta in case of the former. The MacKenzie River delta region is, in terms of extent and formation pattern, the most comparable to the Lena Delta examined in the base study.

The study areas are located in the tundra climate zone, with mean annual air temperatures ranging from around -4°C at the MacKenzie River basin to approximately -11°C measured at Prudhoe Bay (Millot et al., 2003; Kanevskiy et al., 2017). The precipitation in these regions are low with an annual sum of around 150 mm which characterises this area as arid (Pushkareva et al., 2016; Kanevskiy et al., 2017). Apart from the MacKenzie River basin, which partly lies in the discontinuous permafrost zone, all regions are located in the continuous permafrost zone (Figure 1). The climate conditions are comparable to the Lena Delta, which also has a typical High Arctic climate with slightly lower mean annual air temperature (Boike et al., 2013; Nitze and Grosse, 2016).

3 Methods

3.1 Landsat Data

Preprocessing of remote sensing data (Figure 2) was designed along the workflow presented in Nitze and Grosse (2016) and executed in Google Earth Engine, which was also the source of the raw Landsat images. This consisted of the Collection 1/Tier 1 Surface Reflectance Product of the Landsat 5, Landsat 7 and Landsat 8 satellites. All calculations leading up to the final regression data were processed using the Google Earth Engine API.

Three filters were defined for footprint selection:

- overlapping region polygons

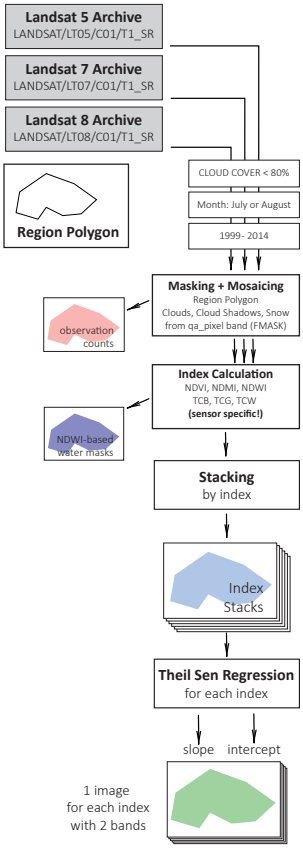

Figure 2. Schematic workflow of processing in Google Earth Engine

- acquisition date 1999 - 2014 and in July or August
- cloud cover less than 80%

Continuous acquisitions during the same orbit split into two or more footprints were compiled into one continuous image. These images were masked if the included QA information indicated a non-surface pixel (cloud cover, cloud shadow or snow cover). If the QA information of two different footprints from the same acquisition disagreed at a pixel in the overlap regions, the pixel was only masked if both footprints indicated a non-surface pixel. The masked mosaics were additionally clipped to the region polygons.

Table 1. Pixel Observation Counts

region	max	stdev	mean
Admirality Bay	90	30.89	39.16
Colville River	100	35.45	44.72
Prudhoe Bay	105	34.26	33.54
Canning River	115	37.34	46.73
Barter Island	110	32.94	59.30
Babbage River	117	42.39	44.63
MacKenzie River	128	42.37	40.19

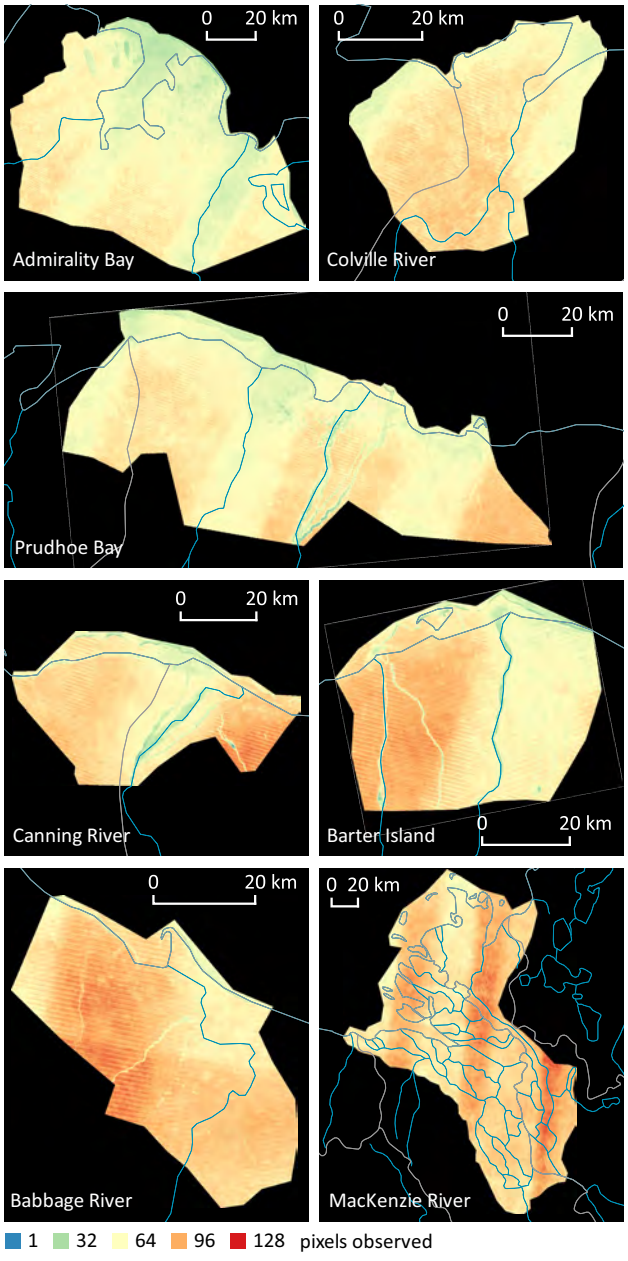

Figure 3. Count of Pixel Observations after QA masking

On average each pixel was observed about 45 times (Table 1) with a slight zonal gradient with lesser observations in the western regions and more observations to the east. There is a high variability in the amount of observations for each region, and the patterns of the broken scan line corrector of Landsat 7 are clearly expressed (Figure 3).

3.2 Preprocessing

3.2.1 Tasseled Cap and Normalized Difference Indices

Resulting surface reflectance images were processed to index images. These were three well-known coefficients of the Tasseled Cap Transformation (Crist, 1985; Huang et al., 2002; Baig et al., 2014) – brightness (TCB), greenness (TCG) and wetness (TCW). The Tasseled Cap coefficients are calculated by multiplying the optical bands with a sensor specific matrix.

A second set of indices consisted of three normalized difference indices, namely the Normalized Difference Vegetation Index (NDVI, Rouse et al. (1974)), the Normalized Difference Water Index (NDWI, as suggested by McFeeters (1996)) and the Normalized Difference Moisture Index (NDMI, Wilson and Sader (2002)). Each index incorporates the normalized difference of two bands, specifically:

$$NDVI = \frac{\rho_{NIR} - \rho_R}{\rho_{NIR} + \rho_R} \tag{1}$$

$$NDWI = \frac{\rho_G - \rho_{NIR}}{\rho_G + \rho_{NIR}} \tag{2}$$

$$NDMI = \frac{\rho_{NIR} - \rho_{SWIR1}}{\rho_{NIR} + \rho_{SWIR1}} \tag{3}$$

The NDVI shows profiles of vegetation canopy greenness, or in our case a metric of tundra greenness. In (1) ρ_R is spectral reflectance in the red band (0.58 to 0.68 μm) where chlorophyll absorbs maximally, and NIR is the reflectance in the near-infrared band (0.73-1.1 μm) where reflectance from the plant canopy is dominant (Markon et al., 1995). Low values of NDVI (lower than or near -0.1) indicate barren land cover or water, whereas higher NDVI values (above 0.1) indicate greenness with lower or higher vegetation canopy (Potter and Alexander, 2020), as well as increased vegetation growth.

The NDMI (Normalized Difference Moisture Index) is largely affected by the amount of moisture on vegetated area and it slightly differs from the NDWI (Normalized Difference Water Index), which represents open water.

The index calculation resulted in six time series over the selected period.

3.2.2 Water Mask

Because region polygons were only roughly delineated and contained stable water surfaces where the trend data indicated changes, a water mask was needed. In particular, as regional aggregates of the trends should reflect processes changing terrestrial surfaces to water and vice versa, the mask should only cover *stable* water surfaces. Multiple approaches are considered in the literature (see Huang et al. (2018)) including algorithms consisting of vegetation and water indices by using certain threshold values or combination of indices with classification. For this study a simple NDWI threshold algorithm was used (McFeeters, 1996). A permanent water pixel was estimated if the 95th percentile of the NDWI values over the period in question had a positive value.

3.2.3 Theil-Sen Trend Calculation

The timeseries were stacked by its respective index and a Theil-Sen Regression (TSR) (Theil, 1992) was applied. The TSR fits a linear model to the time series, using the acquisition date as the regressor and the index value as the response variable, resulting in a slope and intercept coefficient. In contrast to an ordinary least-squares regression, this algorithm is robust against outliers, even if up to 30% of the data are not within the assumed variability (Fernandes and Leblanc, 2005). Google Earth Engine already provides the TSR algorithm, where a time series stack is processed into a single image, with two bands designating the slope and intercept as distinct bands. This implementation however does not give access to the confidence intervals of the regression considered in Nitze and Grosse (2016). Due to the large effort required for a custom implementation of the TSR, it was decided to deviate from the original study in this regard.

3.2.4 Change Pixel Detection

For the subsequent classification of change processes, a randomly selected set of change pixels was needed. This random sampling was restricted to only pixels where the trends suggested a change process. Thus, a further mask was created where the trend data indicated an actual change of the surface characteristics. For this purpose, the regional standard deviation of the trend slopes were calculated to capture their natural variability. A significant change pixel for an index was assumed when its value was outside three standard deviations from a zero trend value. Clusters of change pixels smaller than 9 pixels were not considered as a significant change and removed from the layer.

The index-wise change pixels layers were then combined to a single layer, where a pixel was considered a change pixel if at least one index layer showed a change pixel. 50 random points covered by the change layer were selected and combined with the information of which indices showed a change pixel, and if these were high or low outliers.

3.3 Trend Analysis

The resulting trends, calculated via the TSR, were aggregated for each region to estimate regional slope means and standard deviation (see Appendix D1). TSR intercept means were also calculated, and express the expected value for the trends from

the regression for the last year of the period (2014). Stable water was not considered in these aggregates by employing the NDWI watermasks (see section 3.2.2).

3.4 Change Processes

3.4.1 Erosion & Sedimentation

Sedimentation and erosion processes were found along river courses or coastal sand bars (Figure B1). Erosion describes the ablation of material, sedimentation describes the accumulation of specific soil material. Arctic erosion is also highly influenced by the permafrost in the ground, which is why thermo-related and mechanical erosion occur along ice wedge networks. Thus, the erosion itself is self-amplifying (Jones and Arp, 2015). As sedimentation causes island formations in water bodies it may be accompanied by other change processes like vegetation encroachment. Erosion can be determined when negative trends of NDVI, TCG and TCB trends are found, while sedimentation occurs mostly when negative NDWI, NDMI and TCW trends are calculated (Nitze and Grosse, 2016).

3.4.2 Vegetation Encroachment

Vegetation in permafrost regions of the northern latitudes plays a significant role in the carbon cycle, energy balance and hydrology, and is closely coupled to the state of permafrost. Climate change-induced warming, thawing of the permafrost and increased precipitation result in greening of Arctic regions (Peng et al., 2020). Several studies found positive NDVI trends in a range of Arctic regions (Jia et al., 2003; Walker et al., 2012; Nitze and Grosse, 2016). In this study, change pixels with positive NDVI and TCG trends that were not subject to ice-wedge degradation (3.4.3) were classified as "vegetation encroachment" (Figure B2).

3.4.3 Ice-wedge Degradation

The melting of ground ice and thawing of ice-rich permafrost leads to thermokarst features (Nitzbon et al., 2020). One major type of thermokarst in the continuous permafrost zone is the transition from low-centred to high-centred ice-wedge polygons. This results in the melting of ancient ice-wedges due to repeated frost cracking and ice-vein growth (Nitzbon et al. (2020), Liljedahl et al. (2016)). In contrast to thawing processes in permafrost regions with low ground ice content, thermokarst processes can lead to severe permafrost degradation within a few years and have a landscape-scale impact on carbon decomposition and hydrology. The frozen soil beneath the melting ice-wedges prevents water from draining and leads to the development of deep water-filled troughs (Nitzbon et al., 2020). The formation of these troughs can be observed from satellite images and typically result in positive NDWI and TCW trends, as well as a negative TCB-trend accompanied by rising NDVI and TCG values that are linked to vegetation encroachment in high-centred ice-wedge polygons (Wolter et al., 2016) (Figure B3).

3.4.4 Lake Drainage

Permafrost degradation causes thermokarst lake formations in the Arctic landscape (3.4.3) (Jones and Arp, 2015). 50% to 75% of the Arctic lowlands‘ ice-rich permafrost landscapes are covered by drained thermokarst lake basins (Jones et al., 2012). Lake tapping by rivers, streams, adjacent lakes or ocean, headward gully erosion, anthropogenic influences and thaw slump formations are several factors which cause lakes to drain (Jones and Arp, 2015). Drainage events (example shown in Figure B4) can be analysed by positive NDVI, TCG and TCB trends and negative NDMI , NDWI and TCW trends (Nitze and Grosse, 2016).

3.4.5 Anthropogenic Disturbance

Man-made infrastructure in permafrost regions is not only vulnerable to permafrost thaw induced by climate change, but can itself cause thermokarst processes and thereby accelerate permafrost degradation (Schneider von Deimling et al., 2020). The infrastructure in the continuous permafrost zone is therefore exposed to a particular risk, as is the sensitive landscape, which is threatened by environmental disasters such as oil spills from leaking pipelines (Hjort et al., 2018). In this study, change pixels were assigned to this change class if they were located on newly built infrastructure or were clearly affected by it (example shown in Figure B5). If new infrastructure was built during the study period, positive trends of TCB, as well as negative trends in NDVI, TCG, NDWI, NDMI and TCW were expected. Change pixels that lay on thermokarst features that were apparently induced by nearby infrastructure were assigned to the "Anthropogenic Disturbance" class and typically showed similar trends as described in section 3.4.3.

3.5 Area Estimation of Change Processes

After the classification o f t he 5 0 c hange p ixel i n e ach of the regions, the area share of the different change processes within the study areas was calculated according to (4).

$$A_{CP} = \frac{N_{CP}}{50} \cdot \frac{N_C}{N_{tot}} \cdot 100 \tag{4}$$

A_{CP} is the area share of one change process P in one of the study areas in %, N_{CP} is the number of change pixels of a change process, N_C is the total number of change pixels in one region and N_{tot} is the study area specific total number of pixels.

3.6 Change Process Classification

For the classification, area estimations derived from sample pixels were utilised and then classified with the Random Forest method using the eponymous package in RStudio. Using

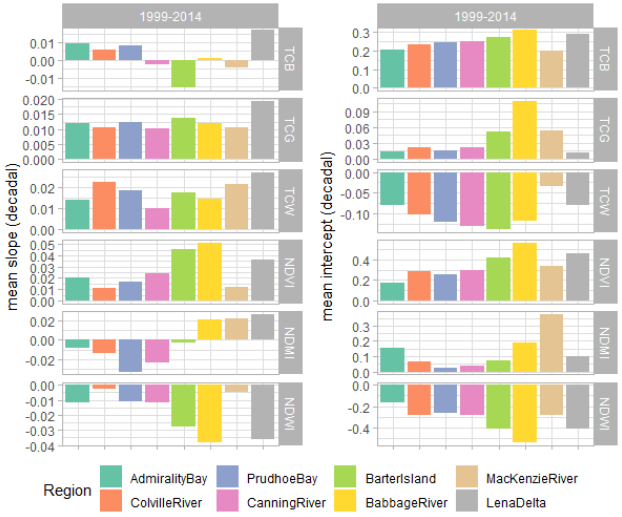

Figure 4. Multi-spectral indices and Tasseled Cap indices for the decadal trends of the slope and intercept means for the whole study area. Lena Delta statistics by Nitze and Grosse, 2016 are included for comparison purposes.

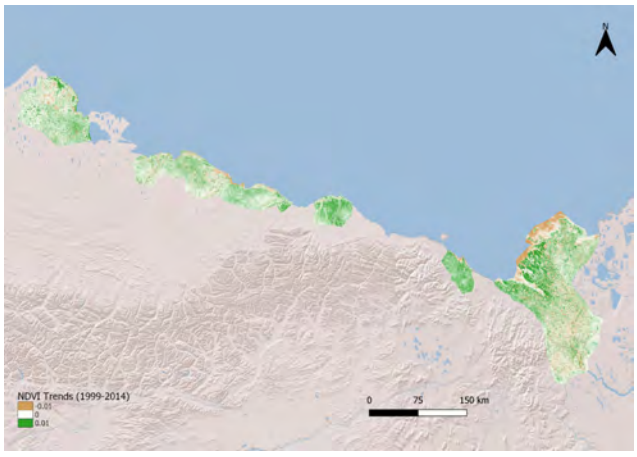

Figure 5. NDVI trends of the slope means for the entire study area.

the area estimation sample points means that the final maps show trend-based classification. This is a useful way of classifying change pixels as it includes many relatively uncorrelated models which operate together as one large committee, which outperforms each individual model. It builds an ensemble of decision trees, which are then trained with the 'bagging' method, which is generally assumed to increase overall accuracies with a combination of learning models. Whilst each 'decision tree' in the 'forest' has its own individual errors, as a group the forest should show less errors as a whole. The chance of greater correct predictions is increased with the number of uncorrelated trees in the model. Once the area estimation maps were classified, pixels not representing a change pixel (as defined in section 3.2.4) were masked out to produce the final products shown section 4.3.

4 Results

4.1 Trend Analysis

In order to explain the effect of climate change on the permafrost of these regions, and to have a direct comparison to the Lena Delta analysis made by Nitze and Grosse (2016), we analyzed the vegetation greenness and moisture contents of the permafrost of these regions with the decadal trends from the TSR for the period 1999 – 2014.

In the following subsections, change patterns and their magnitudes are presented and analyzed. The resulting diagrams for all indices help us identify regional change patterns and behaviors that will further the analysis of the permafrost of the study area (Figure 4).

Greening / Vegetation

There is a general greening trend across the entire study area according to the resulting slope means. The TCG index is similar across all areas of the study region, with a weak positive trend of 0.011 ± 0.001 and no regional patterns observed. The NDVI shows some regional patterns, with the eastern regions exhibiting the highest slope means of around 0.04 and 0.05, and the highest intercepts between 0.04 and 0.05. This indicates higher greening compared to the western areas, but that is not the case for the MacKenzie River which has a slope mean trend of 0.011. (Figure 4 and 5).

Wetness / Moisture

NDWI has a negative correlation compared to the NDVI in terms of slope mean trends for the whole study area. The TCW has a positive correlation with the TCG, but also a negative correlation with the NDMI for the western areas. Its intercept values show a negative trend for all regions, indicating drier surfaces across the whole study area. The NDMI shows some regional patterns, with the Babbage and MacKenzie rivers indicating the only positive slope mean trends (Figure 4 and 6).

Brightness

The TCB exhibits some differential behavior, with no regional patterns observed. Four out of seven regions show a weak positive trend with values less than 0.01, the other three have a weak negative trend. The intercept shows some regional behavior, with a scaling increase from west to east, though it decreases again for the MacKenzie River (Figure 4).

4.2 Change Processes

The area estimations of the change processes (Figure 7) show that the most abundant change processes (besides the "no change" class, which mostly occurred due to falsely identified change pixels on open water areas) in almost all re-

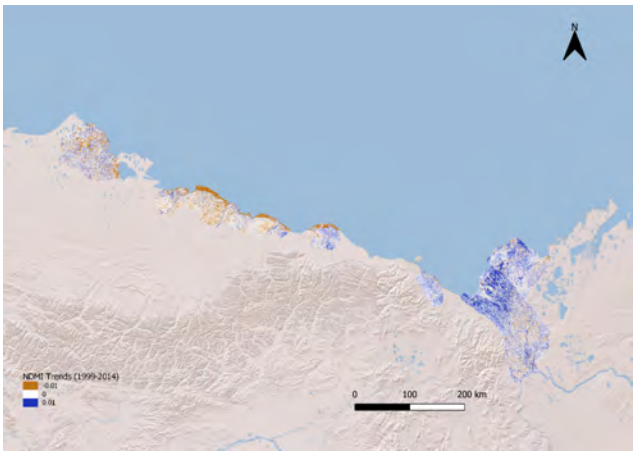

Figure 6. NDMI trends of slope means for the entire study area.

gions are vegetation encroachment and ice-wedge degradation, which are considered to be signs of rising temperatures and thawing (Jia et al., 2003; Nitzbon et al., 2020). Ice-wedge degradation occurred increasingly in regions with many thermokarst lakes, such as Prudhoe Bay, Colville River and the MacKenzie Delta. Greening was especially pronounced in the Barter Island region, Canning River (which had a very distinct area of greening in the eastern part), as well as Prudhoe Bay. Erosion and sedimentation processes, which were mainly found on river banks and at the coast, had overall lower area shares between 0.5% and 1% and 0.2% to 1% respectively. With area shares of typically under 0.5%, lake drainage and anthropogenic disturbance were the least common change processes. As expected, the largest anthropogenic influence was found to be in Prudhoe Bay, which hosts the largest industrial complex in the Arctic (Raynolds et al., 2014).

4.3 Change Process Classification

The results show a variety of success and failures, which will be further discussed later. As shown in Figure 8, there has been a relatively successful classification of the Canning River catchment, with very clear examples of island formation and vegetation encroachment in the eastern region. This validates the earlier analyses, which showed a general greening of the catchment with a high Tasseled Cap Greenness (TCG) value.

Figure C1 shows a partially successful classification of the MacKenzie River basin. Here, excellent sedimentation and erosion processes are shown, with the river clearly highlighted showing the direction of meander development over time. However, artifacts from the satellite imagery have caused confusion in the classification as shown in the top-right image.

Figure C2 shows the Prudhoe Bay region and is a good example of the difficulties of using area estimation points for trend-based classification. As with the MacKenzie River, there are problems with artifacts from the satellite which have interfered with the classification, here these have been identified as anthropogenic disturbance by the classifier. This class was poorly classified in general across all of the regions, for example in the above figure, the airport at Deadhorse was classified as ice-wedge degradation and sedimentation. The reasons for these successes and failures will be further discussed in section 5.3.

5 Discussion

5.1 Trends

There are many factors influencing the trends for permafrost changes, including topography, vegetation, hydrology and disturbances. These factors vary on different timescales and spatial scales (Osterkamp, 2007).

Greening

The summer greening of the study area, which reflects on the increasing slope and intercept of the NDVI values, would be a process of rising summer air and soil temperatures (Berner et al., 2020), but it is not the sole factor. The thermokarst processes over many years, along with the ice-wedge degradation of the lakes of the western areas may result in negative NDVI polygon values (Figure 5). Plant productivity, which is associated with high summer temperatures and summer precipitation, is still dominant. These negative NDVI values may also be a result of anthropogenic disturbances in these areas, especially Prudhoe Bay, and as a result of erosion found along the coastal surfaces of the study area, based on the classification. In general, the greening trends agree with the change process classification.

Moisture

The positive trends in the moisture indices on the Mackenzie river area may be associated, as with the Lena Delta, to over-flooding by the rising of the sea-level, especially on the north-western coastal side of the area. The western areas exhibit some drying, which may be a result of lake drainages or sedimentation according to our classification. Summer precipitation is an important driver of moisture trends, but it is also important to consider the local-scale permafrost thaw which may be a factor of increasing moisture (Liljedahl et al., 2016), so further analysis on a local scale may be required to better interpret these trends.

Lena Delta comparison

The only area showing a consistency with the trend values of the Lena Delta is the MacKenzie River, as they both have many similarities in landscape and water distribution. In general, our study area and the Lena Delta exhibit similar greening in terms of both the TCG and the NDVI, but with no clear pattern for the values of the latter. The coastal processes show a similarity in their pattern with low NDVI values, in-

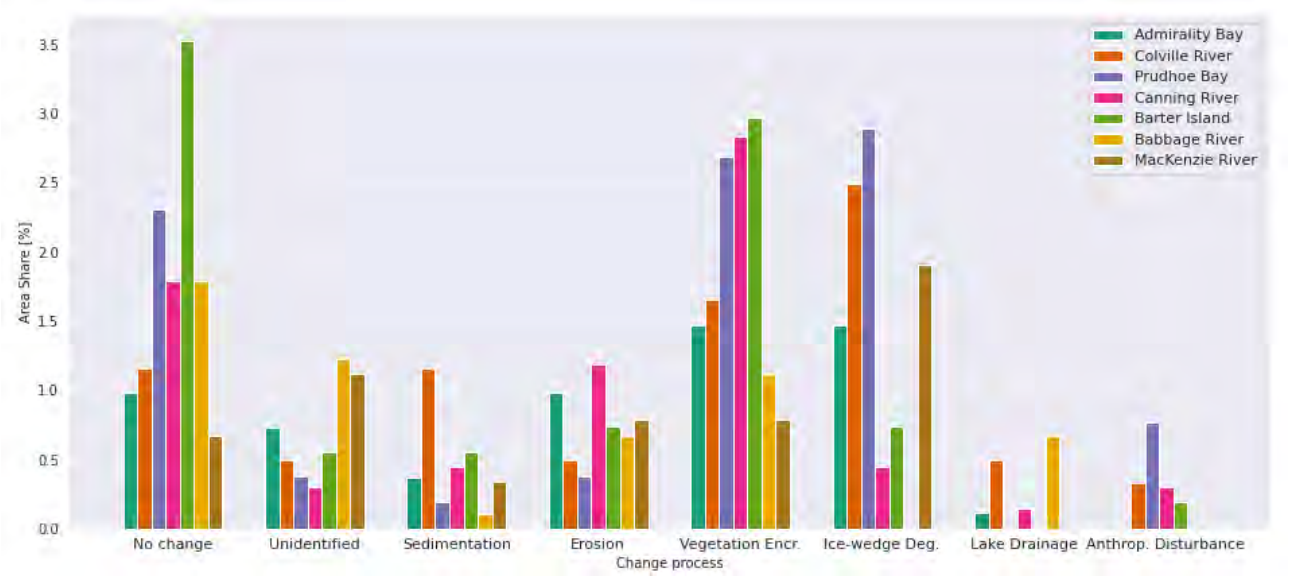

Figure 7. The figure shows the area share in % of each of the change classes in the different study regions.

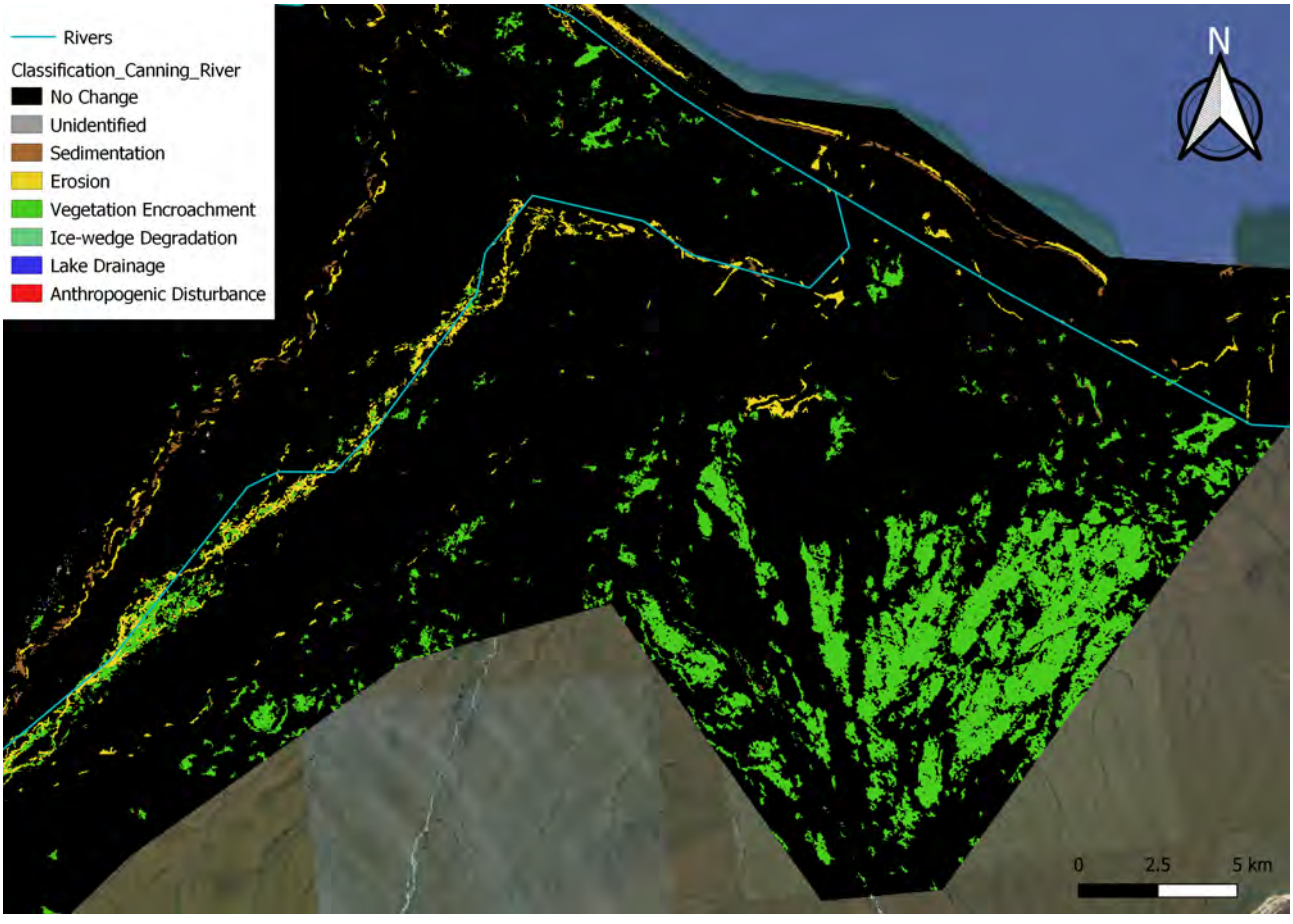

Figure 8. Classification map of Canning River, superimposed on a Google Satellite Hybrid base map, with vegetation encroachment seen clearly in the east of the catchment.

dicating possible sediment deposition and erosion (Nitze and Grosse, 2016). As for the moisture and wetness trends, the magnitude of the MacKenzie River is negatively affecting the results towards the Lena Delta. On-field measurements for inter-comparison are required for a better understanding of these trend findings.

5.2 Change Processes

The classification of the pixels, which was carried out with the help of the tasseled cap and normalized difference indices, as well as the visual interpretation of satellite and aerial images in google earth history, is analysed subjectively and could not be validated due to a lack of ground truth data. Furthermore, the decision for a certain change class was difficult in some cases, because processes such as ice-wedge degradation and vegetation encroachment can overlap and occur at the same point. Reasons for points wrongly classified as change pixels were, among other things, artifacts. These propagated as detector strips from the Landsat images to the index trend maps, as well as areas of water which, due to irregularities such as waves, have triggered strong trends in some of the indices.

5.3 Change Processes Classification

As mentioned in the classification results section, the method of using area estimation points as a base for Random Forest trend-based classification has both positive and negative sides. There are clearly successes shown across the results, insofar that processes, vegetation encroachment in particular, are well-classified. The vegetation encroachment matches the high TCG value for the Canning River, and the sedimentation and erosion processes for the MacKenzie River, respectively. The connotations of this could be profound, as vegetation encroachment may show a melting of permafrost, allowing either a greater variety of vegetation, or just more of the current vegetation type to grow in what is normally a quite barren landscape. As these changes have taken place over time, this could provide proof of climate change in the study area leading to greater vegetation growth on previously bare landscapes (Jia et al., 2009). On the other hand, the failures of the trend-based classification method using area estimation pixels are also apparent. One problematic factor was the artefacts produced by the satellite, obscuring the images used for collecting sample points. These were classified as outliers or non-change pixels and then masked out of the image, resulting in large areas which cannot be analysed. Furthermore, areas of anthropogenic disturbance were also poorly classified, the aforementioned example being the misclassified Deadhorse airport. The main reason for this is the lack of anthropogenic disturbances across the entire region in general, resulting in less samples for this class and therefore greater inaccuracy in using the Random Forest classifier. The solution for both of these main failures could be as simple as collecting more training points, which should provide more examples of anthropogenic disturbance for the classifier to recognise, and therefore improve accuracy. This should be the first point of any future classification research in this area.

6 Conclusions

In this study, we used the Google Earth Engine platform for data acquisition and processing, which proved to be an effective way to create data used in the trend analysis. However, usage of the pre-built Theil-Sen Regression Algorithm made it impossible to study the confidence intervals of the regression, which would help to make statements about the reliability of our results. After working with the API, we are however convinced that it is possible to create a custom implementation of the regression which is also able to provide these metrics.

Applying the presented methods allowed to identify the change processes of the ice-rich landscape. While satellite images allowed the visual estimation of change processes, the indices provided calculated changes which could be used for verification purposes. Change processes on a scale of approximately hundreds of meters up to several kilometers of diameter could be observed in this study.

We were able to confirm the results of Nitze and Grosse (2016) about the greening trend in permafrost regions at the North American Arctic coast. Furthermore, we identified similar patterns of NDVI, TCG and the TCW trends. The NDMI on the other hand hints to subtle differences between the subregions, as the western regions show a notable negative trend.

The most prominent identified change processes during the study period were vegetation encroachment and ice-wedge degradation, which had the highest area share in regions with many thermokarst lakes. Erosion and sedimentation processes were mostly found along river banks and at the coast, while lake drainage events and anthropogenic disturbances were the least common change processes. Though expected that human influences on this landscape would be a very minor change process, our results also do not truly reflect the extent of what anthropogenic disturbances may have actually occurred. This is solely due to the limitations of using 50 sample points to classify change processes. Future research in this area should focus on collecting more training data for more accurate classifications.

References

Baig, M. H. A., Zhang, L., Shuai, T., and Tong, Q.: Derivation of a tasselled cap transformation based on Landsat 8 at-satellite reflectance, Remote Sensing Letters, 5, 423–431, https://doi.org/10.1080/2150704X.2014.915434, 2014.

Beck, I., Ludwig, R., Bernier, M., Lévesque, E., and Boike, J.: Assessing permafrost degradation and land cover changes (1986–2009) using remote sensing data over Umiujaq, sub-arctic Québec, Permafrost and Periglacial Processes, 26, 129–141, 2015.

Berner, L. T., Massey, R., Jantz, P., Forbes, B. C., Macias-Fauria, M., Myers-Smith, I., Kumpula, T., Gauthier, G., Andreu-Hayles, L., Gaglioti, B. V., et al.: Summer warming explains widespread but not uniform greening in the Arctic tundra biome, Nature Communications, 11, 1–12, 2020.

Boike, J., Kattenstroth, B., Abramova, E., Bornemann, N., Chetverova, A., Fedorova, I., Fröb, K., Grigoriev, M., Grüber, M., Kutzbach, L., et al.: Baseline characteristics of climate, permafrost and land cover from a new permafrost observatory in the Lena River Delta, Siberia (1998-2011), Biogeosciences (BG), 10, 2105–2128, 2013.

Brown, J., Ferrians, O. J. J., and Melnikov, E. S.: Circum-arctic map of permafrost and ground ice conditions, Boulder, CO: National Snow and Ice Data Center/World Data Center for Glaciology. Digital media., 1998.

Crist, E. P.: A TM tasseled cap equivalent transformation for reflectance factor data, Remote Sensing of Environment, 17, 301–306, 1985.

Fernandes, R. and Leblanc, S. G.: Parametric (modified least squares) and non-parametric (Theil–Sen) linear regressions for predicting biophysical parameters in the presence of measurement errors, Remote Sensing of Environment, 95, 303–316, https://doi.org/10.1016/j.rse.2005.01.005, 2005.

Fraser, R. H., Olthof, I., Kokelj, S. V., Lantz, T. C., Lacelle, D., Brooker, A., Wolfe, S., and Schwarz, S.: Detecting landscape changes in high latitude environments using landsat trend analysis: 1. Visualization, Remote Sensing, 6, 11 533–11 557, 2014.

Hjort, J., Karjalainen, O., Aalto, J., Westermann, S., Romanovsky, V. E., Nelson, F. E., Etzelmüller, B., and Luoto, M.: Degrading permafrost puts Arctic infrastructure at risk by mid-century, Nature communications, 9, 1–9, 2018.

Hollesen, J., Matthiesen, H., Møller, A. B., and Elberling, B.: Permafrost thawing in organic Arctic soils accelerated by ground heat production, Nature Climate Change, 5, 574–578, 2015.

Huang, C., Wylie, B., Yang, L., Homer, C., and Zylstra, G.: Derivation of a tasselled cap transformation based on Landsat 7 at-satellite reflectance, International journal of remote sensing, 23, 1741–1748, 2002.

Huang, C., Chen, Y., Zhang, S., and Wu, J.: Detecting, Extracting, and Monitoring Surface Water From Space Using Optical Sensors: A Review, Reviews of Geophysics, 56, 333–360, https://doi.org/10.1029/2018RG000598, https://agupubs.onlinelibrary.wiley.com/doi/full/10.1029/2018RG000598, 2018.

IPCC: IPCC Special Report on Climate Change, Desertification, Land Degradation, Sustainable Land Management, Food Security, and Greenhouse gas fluxes in Terrestrial Ecosystems: Summary for Policymakers, 2019.

Jia, G. J., Epstein, H. E., and Walker, D. A.: Greening of arctic Alaska, 1981–2001, Geophysical Research Letters, 30, 2003.

Jia, G. J., Epstein, H. E., and Walker, D. A.: Vegetation greening in the Canadian Arctic related to decadal warming, Journal of Environmental Monitoring, 11, 2231–2238, 2009.

Jones, B. M. and Arp, C. D.: Observing a catastrophic thermokarst lake drainage in northern Alaska, Permafrost and Periglacial Processes, 26, 119–128, 2015.

Jones, M. C., Grosse, G., Jones, B. M., and Walter Anthony, K.: Peat accumulation in drained thermokarst lake basins in continuous, ice-rich permafrost, northern Seward Peninsula, Alaska, Journal of Geophysical Research: Biogeosciences, 117, 2012.

Kanevskiy, M., Shur, Y., Jorgenson, T., Brown, D. R., Moskalenko, N., Brown, J., Walker, D. A., Raynolds, M. K., and Buchhorn, M.: Degradation and stabilization of ice wedges: Implications for assessing risk of thermokarst in northern Alaska, Geomorphology, 297, 20–42, 2017.

Liljedahl, A. K., Boike, J., Daanen, R. P., Fedorov, A. N., Frost, G. V., Grosse, G., Hinzman, L. D., Iijma, Y., Jorgenson, J. C., Matveyeva, N., Necsoiu, M., Raynolds, M. K., Romanovsky, V. E., Schulla, J., Tape, K. D., Walker, D. A., Wilson, C. J., Yabuki, H., and Zona, D.: Pan-Arctic ice-wedge degradation in warming permafrost and its influence on tundra hydrology, Nature Geoscience, 9, 312–318, 2016.

Markon, C. J., Fleming, M. D., and Binnian, E. F.: Characteristics of vegetation phenology over the Alaskan landscape using AVHRR time-series data, Polar Record, 31, 179–190, 1995.

McFeeters, S. K.: The use of the Normalized Difference Water Index (NDWI) in the delineation of open water features, International Journal of Remote Sensing, 17, 1425–1432, https://doi.org/10.1080/01431169608948714, 1996.

Millot, R., érôme Gaillardet, J., Dupré, B., and Allègre, C. J.: Northern latitude chemical weathering rates: clues from the Mackenzie River Basin, Canada, Geochimica et Cosmochimica Acta, 67, 1305–1329, 2003.

Nitzbon, J., Westermann, S., Langer, M., Martin, L. C., Strauss, J., Laboor, S., and Boike, J.: Fast response of cold ice-rich permafrost in northeast Siberia to a warming climate, Nature Communications, 11, 1–11, 2020.

Nitze, I. and Grosse, G.: Detection of landscape dynamics in the Arctic Lena Delta with temporally dense Landsat time-series stacks, Remote Sensing of Environment, 181, 27–41, 2016.

OpenStreetMap contributors: Planet dump retrieved from https://planet.osm.org , https://www.openstreetmap.org, 2017.

Osterkamp, T. E.: Characteristics of the recent warming permafrost in Alaska, Journal of Geophysical Research: Earth Surface, 112, https://doi.org/10.1029/2006JF000578, 2007.

Peng, X., Zhang, T., Frauenfeld, O. W., Wang, S., Qiao, L., Du, R., and Mu, C.: Northern Hemisphere greening in association with warming permafrost, Journal of Geophysical Research: Biogeosciences, 125, e2019JG005 086, 2020.

Potter, C. and Alexander, O.: Changes in Vegetation Phenology and Productivity in Alaska Over the Past Two Decades, Remote Sensing, 12, 1546, 2020.

Pushkareva, E., Johansen, J. R., and Elster, J.: A review of the ecology, ecophysiology and biodiversity of microalgae in Arctic soil crusts, Polar Biology, 39, 2227–2240, 2016.

Raynolds, M. K., Walker, D. A., Ambrosius, K. J., Brown, J., Everett, K. R., Kanevskiy, M., Kofinas, G. P., Romanovsky, V. E., Shur, Y., and Webber, P. J.: Cumulative geoecological effects of 62 years of infrastructure and climate change in ice-rich

permafrost landscapes, Prudhoe Bay Oilfield, Alaska, Global change biology, 20, 1211–1224, 2014.

Rouse, W. J., Haas, H. R., Deering, W. D., Schell, A. J., and Harlan, C. J.: Monitoring the Vernal Advancement and Retrogradation (Green Wave Effect) of Natural Vegetation.[Great Plains Corridor], NASA Technical Report, 1974.

Schneider von Deimling, T., Lee, H., Ingeman-Nielsen, T., Westermann, S., Romanovsky, V., Lamoureux, S., Walker, D. A., Chadburn, S., Cai, L., Trochim, E., Nitzbon, J., Jacobi, S., and Langer, M.: Consequences of permafrost degradation for Arctic infrastructure–bridging the model gap between regional and engineering scales, The Cryosphere Discussions, pp. 1–31, 2020.

Serreze, M. C. and Barry, R. G.: Processes and impacts of Arctic amplification: A research synthesis, Global and Planetary Change, 77, 85–96, https://doi.org/10.1016/j.gloplacha.2011.03.004, 2011.

Theil, H.: A Rank-Invariant Method of Linear and Polynomial Regression Analysis, in: Henri Theil's Contributions to Economics and Econometrics, edited by Raj, B. and Koerts, J., Advanced Studies in Theoretical and Applied Econometrics, pp. 345–381, Springer Netherlands, Dordrecht, https://doi.org/10.1007/978-94-011-2546-8_20, 1992.

Walker, D., Epstein, H., Raynolds, M., Kuss, P., Kopecky, M., Frost, G., Daniëls, F., Leibman, M., Moskalenko, N., Matyshak, G., Khitun, O., Khomutov, A., Forbes, B., Bhatt, U., Kade, A., Vonlanthen, C., and Tichy, L.: Environment, vegetation and greenness (NDVI) along the North America and Eurasia Arctic transects, Environmental Research Letters, 7, 015 504, 2012.

Wilson, E. H. and Sader, S. A.: Detection of forest harvest type using multiple dates of Landsat TM imagery, Remote Sensing of Environment, 80, 385–396, https://doi.org/10.1016/S0034-4257(01)00318-2, 2002.

Wolter, J., Lantuit, H., Fritz, M., Macias-Fauria, M., Myers-Smith, I., and Herzschuh, U.: Vegetation composition and shrub extent on the Yukon coast, Canada, are strongly linked to ice-wedge polygon degradation, Polar Research, 35, 27 489, 2016.

Wulder, M. A., White, J. C., Loveland, T. R., Woodcock, C. E., Belward, A. S., Cohen, W. B., Fosnight, E. A., Shaw, J., Masek, J. G., and Roy, D. P.: The global Landsat archive: Status, consolidation, and direction, Remote Sensing of Environment, 185, 271–283, 2016.

Appendix A: Trend Data

Table A1. Statistics of the trends (1999-2014) of all indices including the slopes (mean and standard deviation) and the intercepts (mean) for the entire study area and the Lena Delta from Nitze and Grosse (2016)

index	statistic	Admirality Bay	Colville River	Prudhoe Bay	Canning River	Barter Island	Babbage River	MacKenzie River	Lena Delta
TCB	Slope Mean	0.0097	0.0056	0.0080	-0.0021	-0.0156	0.0010	-0.0043	0.0168
TCB	Slope StdDev	0.0184	0.0178	0.0188	0.0175	0.0146	0.0136	0.0180	0.0139
TCB	Intercept Mean	0.2042	0.2327	0.2456	0.2504	0.2711	0.3096	0.1968	0.2910
TCG	Slope Mean	0.0119	0.0104	0.0124	0.0102	0.0137	0.0121	0.0105	0.0194
TCG	Slope StdDev	0.0095	0.0085	0.0082	0.0089	0.0096	0.0106	0.0167	0.0139
TCG	Intercept Mean	0.0129	0.0216	0.0165	0.0221	0.0518	0.1098	0.0541	0.0122
TCW	Slope Mean	0.0139	0.0224	0.0184	0.0100	0.0177	0.0144	0.0215	0.0271
TCW	Slope StdDev	0.0179	0.0189	0.0195	0.0177	0.0173	0.0118	0.0188	0.0149
TCW	Intercept Mean	-0.0796	-0.1029	-0.1195	-0.1307	-0.1395	-0.1190	-0.0340	-0.0805
NDVI	Slope Mean	0.0204	0.0107	0.0171	0.0243	0.0452	0.0509	0.0116	0.0359
NDVI	Slope StdDev	0.0504	0.0499	0.0498	0.0411	0.0382	0.0437	0.0765	0.0323
NDVI	Intercept Mean	0.1780	0.2896	0.2550	0.2913	0.4138	0.5594	0.3398	0.4605
NDMI	Slope Mean	-0.0083	-0.0140	-0.0331	-0.0233	-0.0031	0.0211	0.0229	0.0271
NDMI	Slope StdDev	0.0655	0.0611	0.0816	0.0664	0.0664	0.0384	0.0621	0.0413
NDMI	Intercept Mean	0.1544	0.0652	0.0254	0.0410	0.0705	0.1913	0.3771	0.0993
NDWI	Slope Mean	-0.0116	-0.0028	-0.0108	-0.0117	-0.0275	-0.0383	-0.0045	-0.0364
NDWI	Slope StdDev	0.0550	0.0503	0.0523	0.0457	0.0374	0.0436	0.0709	0.0302
NDWI	Intercept Mean	-0.1676	-0.2869	-0.2670	-0.2866	-0.4115	-0.5393	-0.2806	-0.4102

Appendix B: Change Process Examples

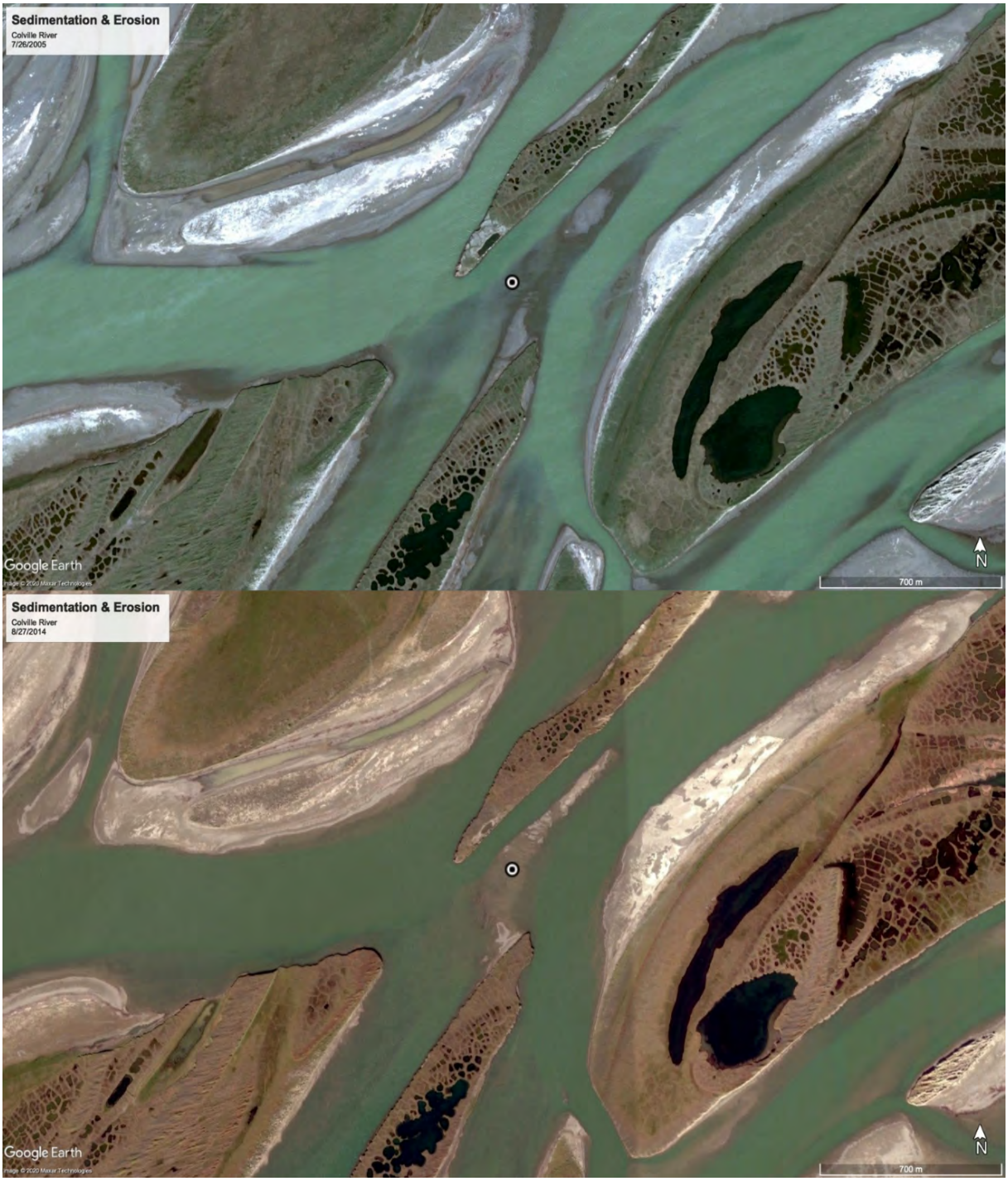

Figure B1. The figure shows multiple ongoing erosion and sedimentation processes at Colville river between 2005 and 2014 (Basemap: Google earth V 7.3.3.7786. (July 26, 2005 & August 27, 2014), http://www.earth.google.com [October 28, 2020]).

Figure B2. The figure shows an area identified as greening/vegetation encroachment between 2005 and 2014 in the Colville river region (Basemap: Google earth V 7.3.3.7786. (July 13, 2005 & August 27, 2014), http://www.earth.google.com [October 28, 2020]).

Figure B3. The figure shows ongoing ice-wedge degradation at a site in Admirality Bay between 2002 and 2011. In 2011 the polygon structure is much more prominent and water seems to be pooling in the polygons (Basemap: Google earth V 7.3.3.7786. (July 31, 2002 & June 18, 2011), http://www.earth.google.com [October 28, 2020]).

Figure B4. The figure shows a lake drainage event between 1999 and 2014 at a site in the Babbage river region (Basemap: Google earth V 7.3.3.7786. (December 31, 1999 & December 31, 2014), http://www.earth.google.com [October 28, 2020]).

Figure B5. The Figure shows the extension of man made infrastructure from 2005 to 2009 at a site in Prudhoe Bay (Basemap: Google earth V 7.3.3.7786. (June 25, 2005 & May 20, 2009), http://www.earth.google.com [October 28, 2020]).

Appendix C: Classification Examples

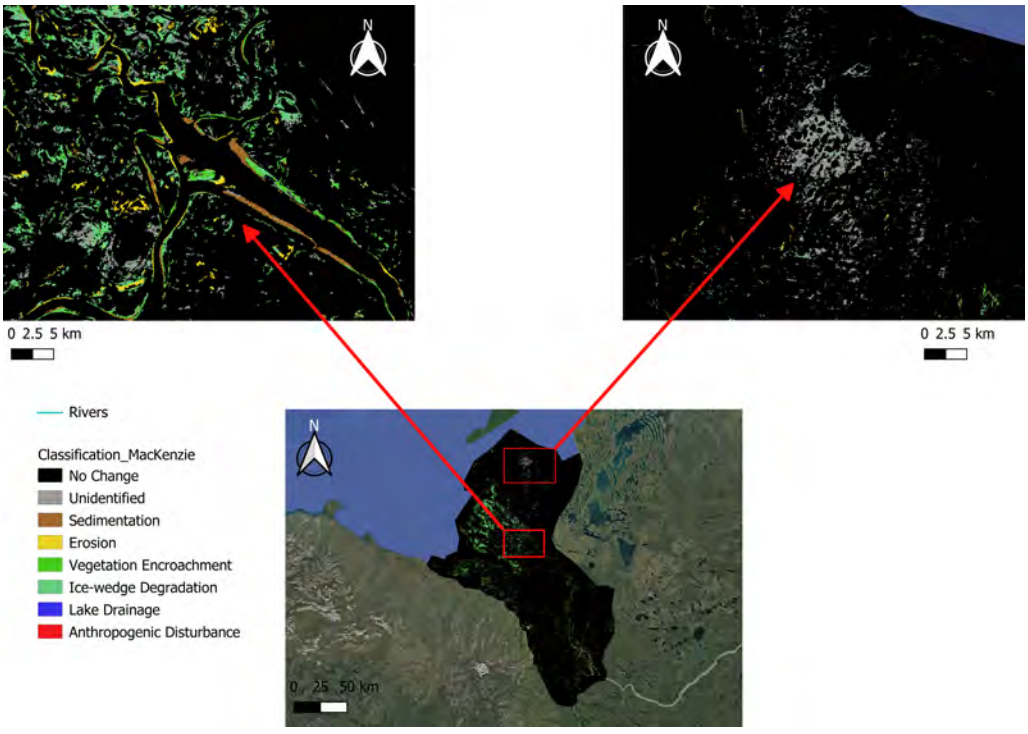

Figure C1. Classification map of the Mackenzie River, superimposed on a Google Satellite Hybrid base map, with good (top left) and poor (top right) classifications shown.

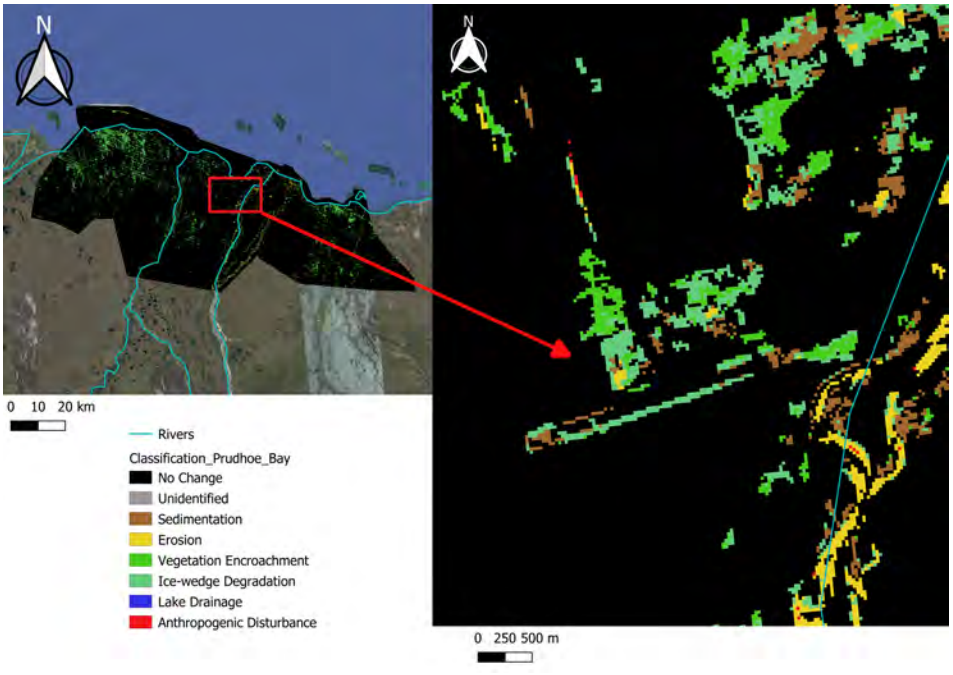

Figure C2. Classification map of Prudhoe Bay, superimposed on a Google Satellite Hybrid base map, and a zoomed in image highlighting classification issues with Deadhorse Airport.

Appendix D: Programming Code

Code for preprocessing in Google Earth Engine is available at
https://code.earthengine.google.com/?accept_repo=users/geograffr/eo_2020_permafrost

D1 R: Trend Analysis

Listing 1. Library Loading and Static Data

```
library(raster)
library(stringr)
library(dplyr)
library(tidyr)

data.dir.1999 = "../trends"

index.labels = c("TCB", "TCG", "TCW", "NDVI", "NDMI", "NDWI")
region.labels = c("AdmiralityBay", "ColvilleRiver", "PrudhoeBay", "CanningRiver",
                  "BarterIsland", "BabbageRiver", "MacKenzieRiver" , "LenaDelta")

lena.delta.df <- data.frame(
  region = "LenaDelta",
  epoch = "1999-2014",
  index = index.labels,
  slope.mean = c(0.0168, 0.0194, 0.0271, 0.0359, 0.0271, -0.0364),
  slope.stdev = c(0.0139, 0.0139, 0.0149, 0.0323, 0.0413, 0.0302),
  intercept.mean = c(0.2910, 0.0122, -0.0805, 0.4605, 0.0993, -0.4102)
)
```

Listing 2. Trend Extraction and Statistics

```
stats.FUN = function(trendfile, watermask) {
  raster.stack <- stack(paste0(trendfile))

  # reproject watermask if necessary:
  if(proj4string(raster.stack) != proj4string(watermask)) {
    watermask = projectRaster(watermask, raster.stack, method = "ngb")
  }

  raster.stack.masked <- mask(raster.stack, watermask, maskvalue = 1)

  data.frame(
    index = str_match(trendfile, "STtrend_([A-Z]+)_")[,2],
    slope.mean = cellStats(raster.stack[[1]], mean) * 10,
    slope.stdev = cellStats(raster.stack[[1]], sd) * 10,
    intercept.mean = cellStats(raster.stack[[2]], mean),
    stringsAsFactors = F
  )
}
```

3. Data File Parsing and Water Mask Extraction

```
calculate.subregions = function(subfolder ,data.dir,  epoch) {
  region.name = str_match(subfolder, "^([A-Za-z]+)(_|$)")[,2]
  subregion.data.folder = paste0(data.dir, "/", subfolder)

  if( region.name == "BabbageRiver" && epoch == "1999-2014") {
    subregion.data.folder = paste0(subregion.data.folder, "/Data/processing_test")
  }

  region.data.files = list.files(
    subregion.data.folder,
    glob2rx("STtrend_*.tif"),
    full.names = T)

  if( length(region.data.files) < 1 ) {
    stop(sprintf("No␣file␣found␣for␣'%s'␣in␣folder␣'%s'",
      region.name, subregion.data.folder
    ) )
  }
  # load the 95perc rasters and create a watermask by
  # using the 95th percentile of the NDWI (band 1) with a positive value:
  watermask.file.name = subfolder

  perc.file = paste0("../watermask/", watermask.file.name, "_perc95_", substr(epoch, 1,4)
,".tif")
  perc.raster = raster(perc.file, band = 1 )
  watermask = perc.raster > 0
  watermask.stats = freq(watermask, useNA = "no")
  watermask.fraction = data.frame(watermask.stats) %>%
     filter(value == 1) %>%
     pull(count)/sum(watermask.stats[,2])
  message(sprintf( "applying␣watermask␣(%.1f%%␣masked␣pixels)", watermask.fraction*100 ))

  results = lapply( region.data.files, stats.FUN, watermask = watermask ) %>%
    bind_rows() %>%
    mutate(region = region.name, epoch = epoch, .before = 1) %>%
    mutate(watermask.fraction = watermask.fraction)
  return(results)
}
```

Listing 4. Master Processing and Data Concatination

```
subfolders = list.files(data.dir.1999, pattern = "^[A-Za-z]+(_[0-9]+)?$")
epoch.results.1999 = lapply(subfolders, calculate.subregions, data.dir.1999, "1999-2014") %>%
  bind_rows()

all.results = epoch.results.1999 %>%
  bind_rows(lena.delta.df) %>%
  mutate(
    index = factor(index, levels = index.labels),
    region = factor(region, levels = region.labels),
    epoch = as.factor(epoch)
  )

all.results %>% filter(epoch == "1999-2014") %>%
  select(-c(epoch, watermask.fraction)) %>%
  pivot_longer(cols = c(slope.mean, slope.stdev, intercept.mean)) %>%
  arrange(index, region) %>%
  pivot_wider(names_from = region)
```